

Virus-Based 3-Dimensional Nanowire Network Copper and Nickel Electrodes

by

Brandon Lew

Submitted to the Department of Materials Science and Engineering in Partial Fulfillment

of the Requirements for the Degree of

Bachelor of Science

at the

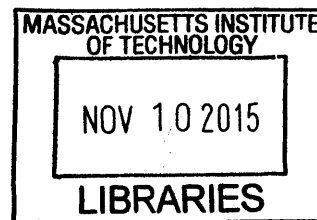
Massachusetts Institute of Technology

June 2011

©2011 Brandon T. Lew

All rights reserved

**ARCHIVES**



The author hereby grants to MIT permission to reproduce and to distribute publicly paper and electronic copies of this thesis document in whole or in part.

**Signature redacted**

Signature of Author.....

Department of Materials Science and Engineering  
May 6, 2011

**Signature redacted**

Certified by.....

Angela M. Belcher  
Germenhausen Professor of Materials Science and Engineering  
Thesis Supervisor

**Signature redacted**

Accepted by.....

Lionel C. Kimerling  
Thomas Lord Professor of Materials Science and Engineering  
Chairman, Undergraduate Thesis Committee

# Virus-Based 3-Dimensional Nanowire Network Copper and Nickel Electrodes

by

Brandon T. Lew

Submitted to the Department of Materials Science and Engineering on May 6, 2011 in partial fulfillment of the requirements for the Degree of Bachelor of Science in Engineering as recommended by the Department of Materials Science and Engineering.

## Abstract

Microbatteries are necessary to powering the next generation of microelectronics. Synthesizing a scalable microelectrode at room temperature is possible using bio-templating. To create a novel 3D electrode, we report M13 virus cross-linking and nickel and copper nanowire synthesis. In this process, virus was cross-linked using glutaraldehyde to form mechanically stable hydrogels, which were then mineralized using electroless deposition. The mineralized hydrogels were of micron-scale thickness with sub-micron pore sizes. SEM and FIB imagery provided visual confirmation of highly-networked nanowires, and EDX demonstrated purity of the nanowires as over 95% pure metal.

Thesis Supervisor: Angela M. Belcher

Title: Virus-Based 3-Dimensional Nanowire Network Copper and Nickel Electrodes

## Acknowledgements

I would like to thank John Burpo for all of his help and guidance on this project. He has been a great graduate student mentor for the past year and a half that I've worked with him, always patient in explaining the problems and listening to the issues. I would also like to thank Professor Belcher for granting me this opportunity to work with John in her lab, where I was always amazed by the exciting progress. Additionally, I'd like to thank all those I worked with in lab, including Tiffany, Nick, Mark, and others. Finally, I'd like to thank my old RA, Bryan, and my friends for assisting me and keeping me on track throughout college.

# Contents

<b>1</b>	<b>Introduction</b>	<b>7</b>
1.1	Motivation for Research . . . . .	7
1.2	Background . . . . .	8
1.2.1	Microbatteries . . . . .	8
1.2.2	Biostructures . . . . .	8
1.2.3	M13 Bacteriophage . . . . .	9
1.2.4	M13 Mineralization . . . . .	10
1.2.5	TMV Mineralization . . . . .	11
1.2.6	Crosslinking and Hydrogels . . . . .	11
<b>2</b>	<b>Experimental</b>	<b>12</b>
2.1	Overview . . . . .	12
2.2	Phage Preparation . . . . .	12
2.2.1	Amplification . . . . .	12
2.2.2	Concentration with Poly(ethylene) glycol . . . . .	13
2.3	Microwell Fabrication . . . . .	13
2.3.1	Polydimethylsiloxane Casting . . . . .	13
2.3.2	Layer-by-layer Film Deposition . . . . .	14
2.4	Hydrogel Formation . . . . .	14
2.4.1	Microwell Hydrogels . . . . .	14
2.4.2	Freestanding Hydrogels . . . . .	15
2.4.3	Hydrogels on Silicon . . . . .	15
2.4.4	Hydrogels on ITO . . . . .	15
2.5	Microstamping . . . . .	16
2.6	Electroless Deposition . . . . .	16
2.6.1	Palladium Sensitization . . . . .	16
2.6.2	Copper Nanowire Mineralization . . . . .	16
2.6.3	Nickel Nanowire Mineralization . . . . .	17
2.7	Imaging . . . . .	17
2.7.1	Atomic Force Microscopy . . . . .	17
2.7.2	Scanning Electron Microscopy . . . . .	17
2.7.3	Focused Ion Beam . . . . .	18

<b>3</b>	<b>Results</b>	<b>19</b>
3.1	Overview . . . . .	19
3.2	Hydrogel Formation . . . . .	19
3.2.1	Microwell Hydrogels . . . . .	19
3.2.2	Freestanding Hydrogels . . . . .	21
3.2.3	Hydrogels on Silicon and ITO Substrates . . . . .	22
3.3	Nanowire Mineralization . . . . .	22
3.3.1	Copper Nanowires . . . . .	22
3.3.2	Nickel Nanowires . . . . .	27
<b>4</b>	<b>Discussion and Conclusion</b>	<b>29</b>
4.1	Overview . . . . .	29
4.2	Hydrogel Control . . . . .	29
4.2.1	Porosity . . . . .	29
4.2.2	Thickness . . . . .	30
4.3	Mineralization Control . . . . .	30
4.3.1	Diffusion Fronts . . . . .	30
4.3.2	Hydrogen Gas Evolution . . . . .	31
4.4	Scalability of Electrodes . . . . .	31
4.5	Future Directions . . . . .	31
4.5.1	Battery Testing . . . . .	31
4.5.2	Mechanical Testing . . . . .	32

# List of Figures

1.1	M13 Bacteriophage model displaying different coat proteins[13]	9
1.2	AFM Phase Images of 2D ordered phage on LbL films	10
1.3	Structure of Glutaraldehyde	11
3.1	SEM Image of 20 $\mu\text{m}$ x 20 $\mu\text{m}$ Nickel Electrodes	20
3.2	SEM Closeup of single 20 $\mu\text{m}$ x 20 $\mu\text{m}$ Nickel Electrode	21
3.3	Freestanding Hydrogel	21
3.4	SEM Image of Copper Nanonetwork on Silicon	23
3.5	SEM Image of Freestanding Copper Nanonetwork Cutaway	24
3.6	EDX of Copper Nanonetwork	24
3.7	FIB Image of Copper Nanonetwork showing Burn-through	25
3.8	FIB Image of Copper Nanowires	26
3.9	SEM Crosssection Image of single Copper Nanowires	26
3.10	SEM Image of Nickel Nanonetwork	27
3.11	SEM Image of Freestanding Nickel Nanonetwork Cutaway	28
3.12	EDX of Nickel Nanonetwork	28

# Chapter 1

## Introduction

### 1.1 Motivation for Research

The motivation behind this thesis is microbattery engineering. The proliferation of small-scale electronics in everyday devices is limited in part by the availability of small, portable batteries. Micro-electronics require little energy to run, and existing batteries are orders of magnitude larger than the actual electronics. In order to construct microbatteries, new methods of fabricating battery components have been developed to make scalable batteries at tabletop chemistry conditions. The novelty that this research introduces is the use of viruses to create 3D porous nanonetworks that can be mineralized into electrodes. This chapter will discuss current techniques in microbattery fabrication, uses of biological structures in microbattery design, and new 3D crosslinking techniques.

## 1.2 Background

### 1.2.1 Microbatteries

Microbatteries are defined as batteries smaller than today's coin cell batteries. On the upper size bound, this means a maximum diameter of approximately 5 mm, as found in standard hearing aid batteries. Their major potential use is in microelectronics, where the energy requirement is very low and size is often a more important design constraint. Microbatteries have been constructed using lithography[1], layer-by-layer deposition[2], electroplating[3], and micromachining[4]. Efforts have also been made at creating machined 3D electrodes using constructed posts[5, 6]. All of these techniques are costly when creating fine structures at the nano- and micro- scale. Additionally, they are machine and time intensive, and battery components are often created in harsh environments.

### 1.2.2 Biostructures

Biological-based nanostructures hold great promise for microbatteries. Biological molecules can be easily modified to suit an environment or to express a specific binding affinity. The same molecules also act as building blocks for nano-scale engineering by self-assembling into ordered structures. Additionally, most chemistry with biological molecules can be conducted at tabletop conditions. Biological molecules such as functionalized DNA, viruses, and proteins have been used to make transistors[7], biosensors[8], and memory devices[9] for microelectronics. In the field of microbattery research, two different viruses, Tobacco Mosaic Virus (TMV) and M13 bacteriophage, have successfully been templated to form ordered 2-D monolayers[10, 11]. Nanowires of electrode material have been mineralized on these monolayers. This research utilized the M13 bacteriophage exclusively for nanostructure fabrication.



### 1.2.3 M13 Bacteriophage

M13 is a filamentous bacteriophage consisting of a protein capsid surrounding a single-stranded DNA genome[12]. The phage selectively infects *Escherichia coli* bacteria by attaching to a conjugative pilus. The virus inserts its genomic material into the cell during infection. The cell is co-opted into producing additional copies of the viral genome and proteins using bacterial enzymes. The phage is constructed within the outer membrane of the *E. coli* cells and secreted once completed. The whole viral life-cycle of infection, copying, and secretion is a non-lytic process.

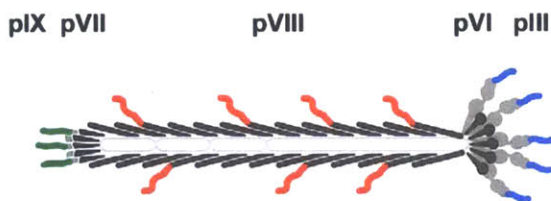


Figure 1.1: M13 Bacteriophage model displaying different coat proteins[13]

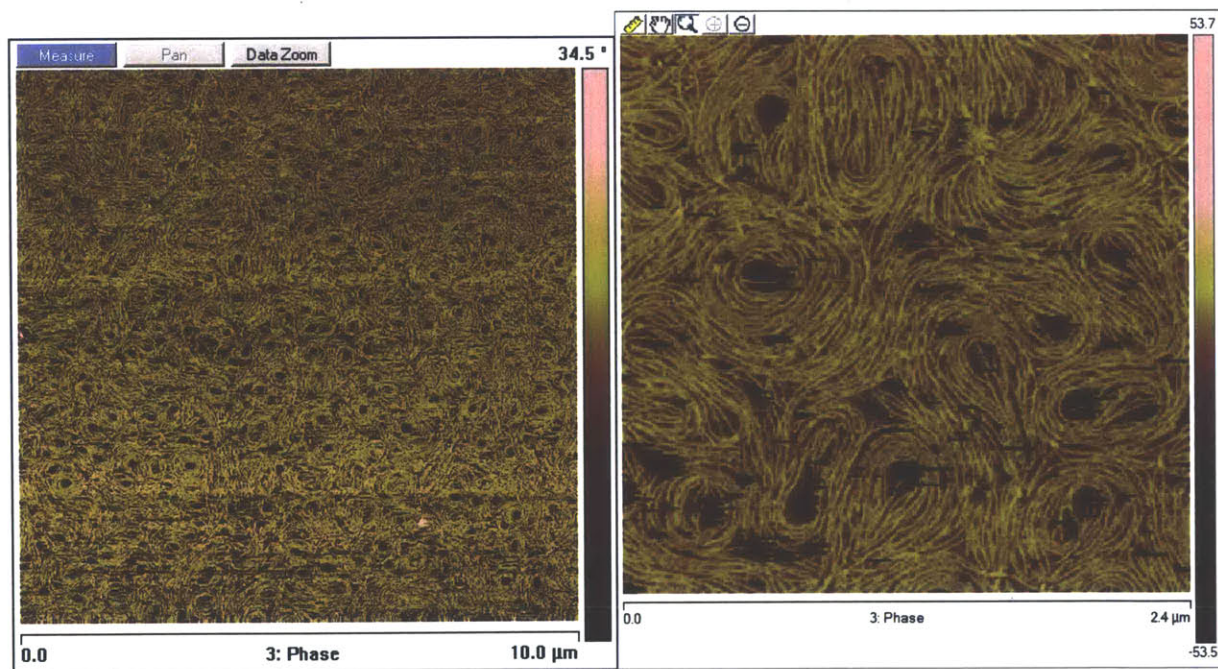
The capsid is primarily composed of 2,700 copies of the major coat protein, p8. Attached at the ends of the phage coat are four different minor coat proteins, p3, p6, p7, and p9. Figure 1.1 displays how the different coat proteins are arranged on the outer surface of the capsid. The terminal side containing P3 is the end which attaches to and infects *E. coli* cells. A single phage is approximately 6 nm in diameter and 900 nm in length. The high-surface area to volume ratio and long, flexible rod-like structure make this phage ideal for creating porous networks and mineralizing electrode materials.

This study used a particular strain of M13 bacteriophage known as E3. E3 is a modified M13 virus that has an triglutamate-aspartate (EEED-) attached to the N-terminus of each p8 protein. The four added amino acid residues are stuck to the outside of the protein capsid, giving the E3 strain enhanced ability to bind cations compared to wild-type M13. E3

was selected for this project because of previously demonstrated ability by a related clone, tetraglutamate (E4), and a mix of E4/E3 clones to bind metal cations during nanowire formation[14].

### 1.2.4 M13 Mineralization

Previous research with M13 has resulted in mineralization of electrode nanowires on 2-D ordered monolayers of phage. These monolayers were atop charged polymer layer-by-layer (LbL) films of linear poly(ethylene imine) (LPEI) and poly(acrylic acid) (PAA)[15]. The bottom and surface layers were LPEI, which promoted phage binding through the negatively-charged EEED- group on the *N*-terminal end of the p8 protein.



(a) Wide view

(b) Closeup

Figure 1.2: AFM Phase Images of 2D ordered phage on LbL films

Figure 1.2 shows how the phage orders on a 12.5 layer LbL film. Electrode materials such

as gold nanoparticles[14], cobalt oxide[16], and iron phosphate[17], have been mineralized on 2D ordered phage and phage in solution.

### 1.2.5 TMV Mineralization

Previous research with the tobacco mosaic virus, similar in size to M13 but a rigid rod virus, has involved affixing the virus upright to a gold substrate[18]. Electrode materials such as nickel[19], gold[20], and copper[21] have been mineralized onto the viruses using electroless deposition (ELD). In electroless deposition, metals are reduced from an aqueous solution without the use of an external current. Hydrogen gas is evolved by a reducing agent, which causes the positively-charged metal ions to mineralize on the surface of the TMV. Electroless deposition is simple and easy to control. This research used electroless deposition to mineralize phage structures.

### 1.2.6 Crosslinking and Hydrogels

Glutaraldehyde  $\text{CH}_2(\text{CH}_2\text{CHO})_2$  is an organic compound commonly used to cross-link proteins. Figure 1.3 displays glutaraldehyde in its most stable conformation, consisting of two aldehyde groups connected by three carbons. While the exact mechanism of crosslinking is not known[22], glutaraldehyde has been used previously to crosslink M13 phage[23]. Glutaraldehyde is able to connect the p8 proteins of the E3 strain together. Given the numerous p8 proteins on each M13, glutaraldehyde was selected to cross-link phage for hydrogels.

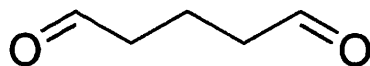


Figure 1.3: Structure of Glutaraldehyde

# Chapter 2

## Experimental

### 2.1 Overview

Hydrogel formation and mineralization was the main focus of this research. E3 phage was concentrated and pipetted onto a variety of substrates. Glutaraldehyde was added to cross-link the phage, forming hydrogels. Hydrogels were then sensitized with palladium and electrodeless deposition reactions were performed to mineralize the network with electrode material. This chapter will discuss the methods used to create phage hydrogels and mineralize them into electrodes. The exact methods discussed are the final methods used to in this research.

### 2.2 Phage Preparation

#### 2.2.1 Amplification

The E3 phage was amplified from existing stock using the ER2738 strain of *E. coli*. It was prepared in large 1L batches, and DNA sequencing was performed to ensure that the EEED- functional group was still expressed by the major coat p8 protein. After amplification, concentrations of E3 were quantified using a Nanodrop ND-1000 spectrophotometer.

Concentrations were on the order of  $1e13$  plaque-forming unit (pfu)/mL. Phage was stored at  $4\text{ }^{\circ}\text{C}$  in phosphate-buffered saline (PBS) until used.

### **2.2.2 Concentration with Poly(ethylene) glycol**

In order to create stable hydrogels, the phage was concentrated with the use of poly(ethylene) glycol (PEG). One mL of phage stock from amplification was pipetted into microcentrifuge tubes. Next,  $167\text{ }\mu\text{L}$  of PEG was added to each of the microcentrifuge tubes, and the tubes were stored at  $4\text{ }^{\circ}\text{C}$  for 4 h. The PEG caused the phage to precipitate out of the PBS. The phage was spun down at 14,000 rpm for 10 min using a tabletop microcentrifuge, and the supernatant removed. The pellet was dissolved in  $50\text{ }\mu\text{L}$  of PBS per tube and recollected. Phage was stored at  $50\text{ }^{\circ}\text{C}$  for 20 min to break up phage aggregates via thermal agitation and then quantified using a Nanodrop ND-1000 spectrophotometer. Concentrated phage was on the order of  $1e14$  pfu/mL.

## **2.3 Microwell Fabrication**

### **2.3.1 Polydimethylsiloxane Casting**

Polydimethylsiloxane (PDMS) was cast over etched silicon masters to create a flexible substrate for creating micron-scale electrode "pads." Etched silicon masters were obtained from Forrest Liao with "pads" of cross-sectional dimension  $20\text{ }\mu\text{m} \times 20\text{ }\mu\text{m}$  and depth of  $6\text{ }\mu\text{m}$ . PDMS was cast over these masters to create well features in the polymer. Sylgard®184 was mixed in a standard 10:1 (m/m) solution of silicone elastomer base:curing agent for 15 min. The solution was poured over the silicon masters and dessicated to remove air bubbles. The PDMS was then baked at  $80\text{ }^{\circ}\text{C}$  overnight to crosslink the polymer. A  $2\text{ cm} \times 7\text{ cm}$  slab, including the featured surface, was removed from the PDMS cast.

### **2.3.2 Layer-by-layer Film Deposition**

PDMS substrates were covered in a 30.5 layer-by-layer LbL film of LPEI/PAA. PDMS substrates were blown with  $N_2$  gas to remove particulate matter. They were then plasma cleaned for 1 min on medium setting. Solutions of 0.02M LPEI and 0.02M PAA were adjusted to pH 5. The PDMS was dipped in LPEI for 15 min and then three successive 1 min DI water baths followed by dipping in PAA for 15 min and then three more successive 1 min DI water baths until a LbL film of 30.5 bilayers was produced.

## **2.4 Hydrogel Formation**

Hydrogels were created by cross-linking phage to itself. The gels were created inside microwells on PDMS substrates, as freestanding gels, and fixed on silicon and indium tin oxide (ITO) coated polyethylene terephthalate (PET) substrates.

### **2.4.1 Microwell Hydrogels**

For microwell hydrogels, the featured portion of the PDMS substrate was cut away. DI water was added on top of the PDMS, and the substrate was slightly agitated for 5 min. A dialysis membrane was cut to fit over the substrate, placed on top, agitated to shear off excess DI water, and removed. 20 mL of concentrated phage was placed on top of the PDMS, and the dialysis membrane was placed back on top and agitated to shear off excess phage. The PDMS substrate was placed feature-side down in 50% glutaraldehyde for 5 min. The PDMS was then placed in 50 mL DI water to remove excess glutaraldehyde.

### **2.4.2 Freestanding Hydrogels**

For freestanding hydrogels, 100-200  $\mu\text{L}$  of concentrated phage was placed in a microcentrifuge tube. 500  $\mu\text{L}$  of 50% glutaraldehyde was pipetted to the bottom of the tube. The gels sat for 1.5h, at which time the gel was removed using tweezers and placed in 50 mL of DI water to let excess glutaraldehyde diffuse out of the gel.

### **2.4.3 Hydrogels on Silicon**

For fixed hydrogels on silicon, 1 cm x 1 cm Si squares and 0.7 cm x 0.7 cm dialysis membrane squares were cut. For each sample, 10  $\mu\text{L}$  of phage was placed on the center of the Si square. The dialysis membrane square was placed on top of the phage and 50% glutaraldehyde was added on top of the membrane until the glutaraldehyde meniscus covered the entire membrane. The gels sat for 1.5h, at which time the samples were placed, with membranes still affixed, in 50 mL of DI water to remove excess glutaraldehyde. After the gel was rinsed, the dialysis membrane was removed.

### **2.4.4 Hydrogels on ITO**

For fixed hydrogels on ITO, 2 mm thick squares of styrene-butadiene rubber with 8 mm diameter holes was placed atop ITO-coated PET and a glass slide. The entire assembly was affixed with two alligator clips. 100  $\mu\text{L}$  of phage was added into the rubber well. The assembly was placed upside down in 50% glutaraldehyde for 1.5h and then repeatedly rinsed in DI water. The ITO with hydrogel was then removed from the assembly and placed in 50 mL DI water to remove excess glutaraldehyde.

## 2.5 Microstamping

Following the deposition of hydrogels in microwells, the hydrogel "pads" were transferred to ITO. ITO substrates were plasma cleaned on high for 3 min to induce a surface charge. The ITO sandwiched between a PDMS substrate containing hydrogel "pads" and a glass slide and affixed using binder clips. The assembly was baked at 50 °C for 20 min. The assembly was then removed and the PDMS carefully peeled off the ITO.

## 2.6 Electroless Deposition

### 2.6.1 Palladium Sensitization

Samples were placed in 10 mM  $\text{Na}_2\text{PdCl}_4$  adjusted to pH 7 for 1.5h to diffuse  $\text{PdCl}_4^-$  ions throughout the gel. The palladium acted as a catalyst to favor the future electroless deposition. Samples were then placed in 0.1M dimethylaminoborane (DMAB) for 1h. The DMAB reduced the palladium around the virus. Samples were then rinsed in DI water for 45 min to remove excess palladium and DMAB.

### 2.6.2 Copper Nanowire Mineralization

Following palladium sensitization, gels were placed in 10 mL  $\text{ELD}_{\text{Cu}}$  solutions minus the reducing agent ( $\text{ELD}_{\text{Cu}}^*$ ) for 1 h.  $\text{ELD}_{\text{Cu}}^*$  consisted of 0.1M  $\text{CuSO}_4$ , 0.25M glycine, and 0.5M 2-(*N*-morpholino)ethanesulfonic acid (MES) and was adjusted to pH 7. Gels were then immediately transferred to 10 mL of  $\text{ELD}_{\text{Cu}}$ .  $\text{ELD}_{\text{Cu}}$  consisted of 0.1M  $\text{CuSO}_4$ , 0.25M glycine, 0.5M MES, and 0.1M DMAB and was adjusted to pH 7. Gels were incubated in  $\text{ELD}_{\text{Cu}}$  for approximately 1 h, or until the gels had turned a coppery color.



### **2.6.3 Nickel Nanowire Mineralization**

Following palladium sensitization, gels were placed in 10 mL  $\text{ELD}_{\text{Ni}}$  solutions minus the reducing agent ( $\text{ELD}_{\text{Ni}}^*$ ) for 1 h.  $\text{ELD}_{\text{Ni}}^*$  consisted of 0.1M  $\text{NiSO}_4$ , 0.25M glycine, and 0.5M MES and was adjusted to pH 7. Gels were then immediately transferred to 10 mL of  $\text{ELD}_{\text{Ni}}$ .  $\text{ELD}_{\text{Ni}}$  consisted of 0.1M  $\text{NiSO}_4$ , 0.25M glycine, 0.5M MES, and 0.1M DMAB and was adjusted to pH 7. Gels were incubated in  $\text{ELD}_{\text{Ni}}$  for approximately 5 min, or until gels had turned black with a hint of silver throughout.

## **2.7 Imaging**

### **2.7.1 Atomic Force Microscopy**

In atomic force microscopy (AFM), a tiny cantilever is rasterized across the surface of the sample. By measuring the movement of a laser reflected off the top of the cantilever, an image of the surface is constructed. A feedback loop is used to shift the sample vertically in order to maintain constant cantilever deflection, thus generating a height profile for the sample. Tapping mode AFM was conducted and data collected on a NanoScope IV and VIII.

### **2.7.2 Scanning Electron Microscopy**

In scanning electron microscopy (SEM), an electron beam is rasterized over the surface of a sample. Detectors collect the secondary electrons that result from inelastic collisions and back-scattered electrons that result from elastic collisions. This data is used to generate a high-magnification image of the sample based on surface conductivity in the case of secondary electrons and regions of differing atomic mass in the case of back-scattered electrons. Characteristic X-rays are also collected by a detector. Energy-dispersive X-ray spectroscopy

(EDX) is used to determine the elemental composition of the sample based on X-ray energy. SEM was conducted in the Center for Materials Science and Engineering (CMSE) located in Building 13. John Burpo scanned all samples for this research using a JOEL 6320FV High-Resolution SEM.

### **2.7.3 Focused Ion Beam**

In focused ion beam etching (FIB), an ion beam is rasterized over the surface of the sample, much like as in SEM. The ions are much heavier and slower than electrons of the same energy level, and therefore do not penetrate as deeply. Detectors collect the secondary ions from collisions and create a high-magnification image of the sample. FIB is also used at high ion currents to etch through the sample, demonstrating depth and internal structure of the sample. FIB was conducted in CMSE. John Burpo scanned all samples for this research using a Helios Nanolab 600 Dual Beam FIB Milling System.

# Chapter 3

## Results

### 3.1 Overview

Hydrogels were successfully created on all substrates. Copper and nickel nanowires of diameters from 80-100  $\mu\text{m}$  were mineralized on hydrogels. SEM and FIB imagery indicated that mineralized hydrogels had sub-micron to micron pore sizes. EDX indicated that metal nanowires were of over 95% purity.

### 3.2 Hydrogel Formation

#### 3.2.1 Microwell Hydrogels

Efforts to create phage hydrogels inside microwells were partially successful. The microwells were filled with crosslinked phage, and the phage was successfully stamped onto ITO substrates. However, the quantity of phage overgrew the size of the wells and separate phage pads grew together.

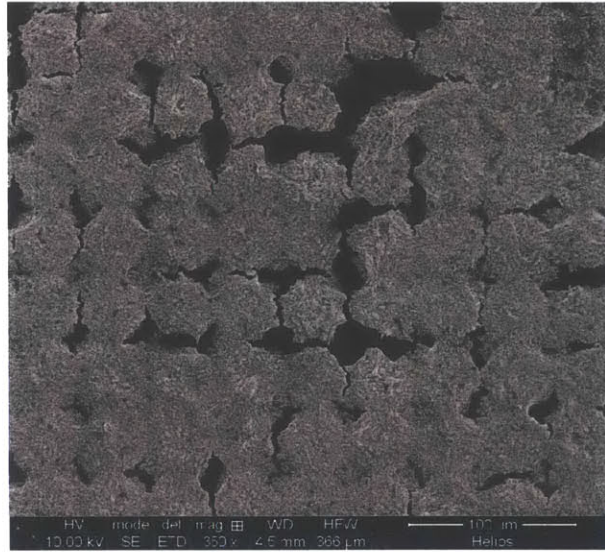


Figure 3.1: SEM Image of 20  $\mu\text{m}$  x 20  $\mu\text{m}$  Nickel Electrodes

Figure 3.1 shows a large patch of phage pads after with nickel. Most of the phage pads have overgrown and are connected to neighboring pads, but there are some unconnected pads. Figure 3.2 shows a single pad which is partially connected to neighboring pads. The center pad is unconnected to the pads to the top and to the bottom. There are phage bridges connecting the center pad to the pads to the left and to the right. The thin nature of the bridges is demonstrated by the cleavage in the bridge connecting the center and right pad. Overall, the phage pads were roughly square, like the microwells they were created in.

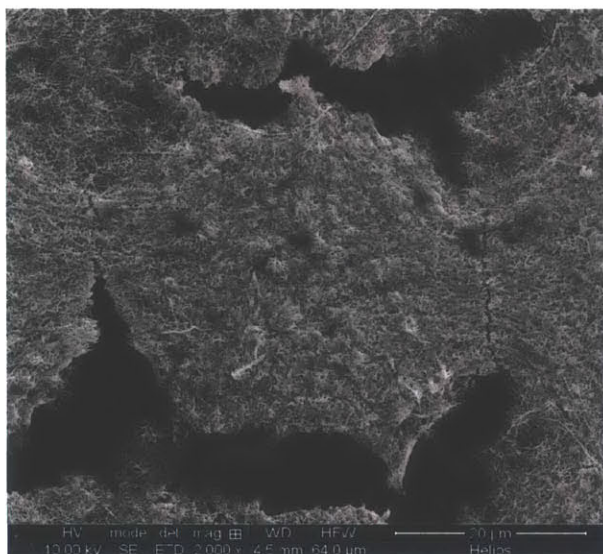


Figure 3.2: SEM Closeup of single  $20\ \mu\text{m} \times 20\ \mu\text{m}$  Nickel Electrode

### 3.2.2 Freestanding Hydrogels

As crosslinking occurred, the phage solution atop the glutaraldehyde lost optical clarity. Figure 3.3 shows a freestanding hydrogel. The hydrogel was no longer transparent and had a whitish cast. The hydrogel was mechanically stable outside of an aqueous environment and manipulable using laboratory tweezers. AFM was attempted using the conditions above, but was inconclusive.

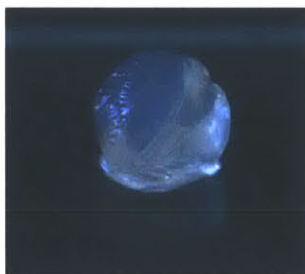


Figure 3.3: Freestanding Hydrogel

### **3.2.3 Hydrogels on Silicon and ITO Substrates**

Hydrogels created on silicon and ITO were visible when substrates were removed from water. Substrates only remained wetted where hydrogels existed. Hydrogels were clear with a slight whitish cast.

## **3.3 Nanowire Mineralization**

Following palladium mineralization, phage hydrogels turned brown as the palladium diffused into the network. Slicing hydrogels demonstrated that palladium had diffused throughout the thickness of the gel.

### **3.3.1 Copper Nanowires**

Palladium-sensitized hydrogels reacted slowly when placed in the ELD solution. Reduction of copper onto the phage slowly caused the evolution of hydrogen gas. Hydrogen gas that evolved on the inside of the hydrogel cause freestanding hydrogels to float to the top of the solution. At around 1 h, the hydrogel turned a coppery color. Further deposition resulted in copper plating over the virus network. The samples imaged were removed after incubating in the ELD solution for approximately 1 h.

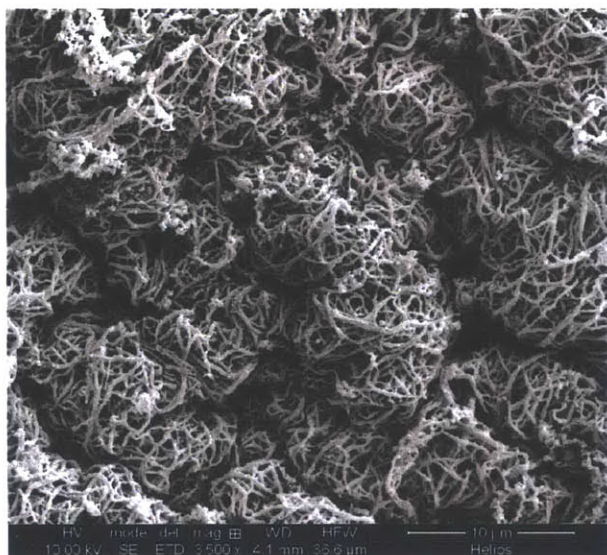


Figure 3.4: SEM Image of Copper Nanonetwork on Silicon

Figure 3.4 shows a top view of the exterior of a copper nanowire network on a silicon substrate. The phage has mineralized all over the network. In the top left corner, large nodules of copper have mineralized, which is the precursor to copper plating over the sample. Figure 3.5 shows a side SEM view of a cutaway of a freestanding copper nanowire network. The image shows the mineralization of the phage over the whole interior of the phage network, which is over  $30\ \mu\text{m}$  thick.

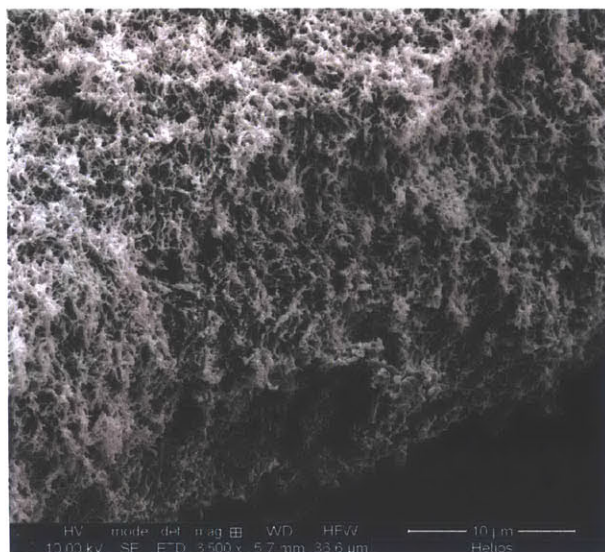


Figure 3.5: SEM Image of Freestanding Copper Nanonetwork Cutaway

Figure 3.6 is the EDX of a copper sample. The EDX shows that copper-mineralized hydrogels have mineralized with over 95% copper, resulting in high-purity nanowires.

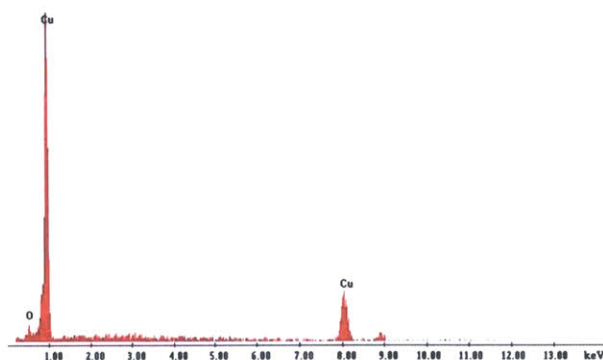


Figure 3.6: EDX of Copper Nanonetwork



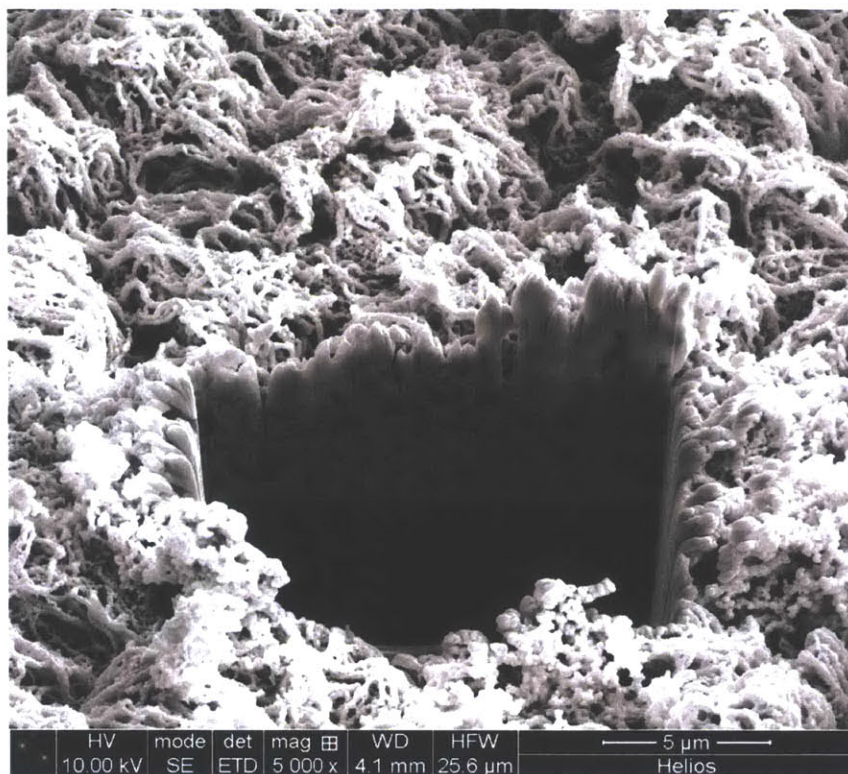


Figure 3.7: FIB Image of Copper Nanonetwork showing Burn-through

Figure 3.7 shows a FIB image of a copper nanowire network on a silicon substrate. The phage network is approximately  $5 \mu\text{m}$  thick and fully mineralized throughout. The FIB was used to burn through the sample down to the substrate. The resulting sidewalls in the center demonstrate the mineralization and pore size in the center of the phage network. Figure 3.8 is a closeup FIB image of nanowires. This image shows how nanowires mineralize, with nucleation at numerous sites along the length of the capsid until the phage is fully mineralized.

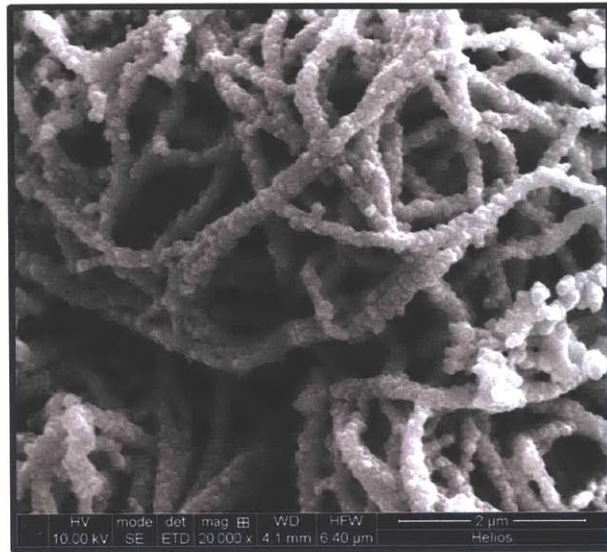


Figure 3.8: FIB Image of Copper Nanowires

Figure 3.9 shows a few copper nanowires at high magnification under SEM. The nanowire is approximated  $80 \mu\text{m}$  in diameter. The small center of the nanowire is dark where the phage is, as the  $6 \mu\text{m}$  phage capsid is non-conductive.



Figure 3.9: SEM Crosssection Image of single Copper Nanowires

### 3.3.2 Nickel Nanowires

Palladium-sensitized hydrogels reacted vigorously when placed in the ELD solution. DMAB-facilitated reduction of the nickel was rapid, and the hydrogel turned black at around 1 min. Hydrogen gas evolved on both the outside and inside of the hydrogel. Trapped hydrogen bubbles caused freestanding hydrogels to float to the top of the solution. At around 20 min, pure nickel plated over the virus network, turning the exterior of the hydrogel silver. The samples imaged were removed after incubating in the ELD solution for approximately 5 min.

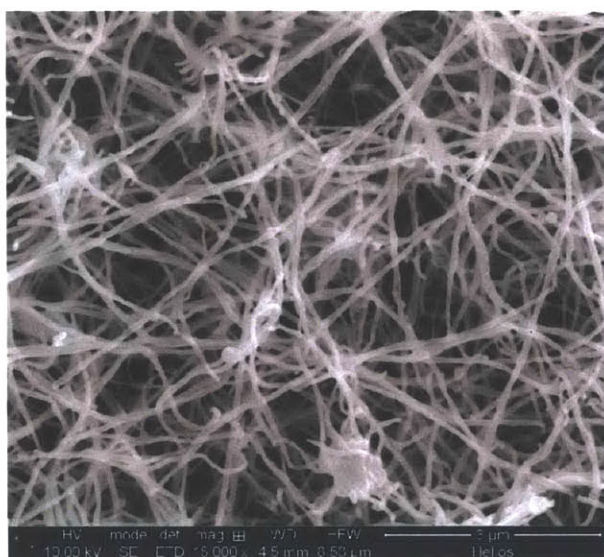


Figure 3.10: SEM Image of Nickel Nanonetwork

Figure 3.10 displays a closeup SEM view of nickel nanowires. The nanowires that have mineralized are about 100 nm in diameter. The porous nature of the network is also obvious, with pores on the order of 1  $\mu\text{m}$  wide. Figure 3.11 shows a SEM side view of a freestanding nickel hydrogel. The thickness of the mineralized hydrogel is approximately 17  $\mu\text{m}$  after drying. The nanowires have variable thickness going vertically throughout the sample. Nanowires on the top, originally the exterior of the hydrogel, are thicker than nanowires on the bottom of the image, which were originally on the interior of the hydrogel.

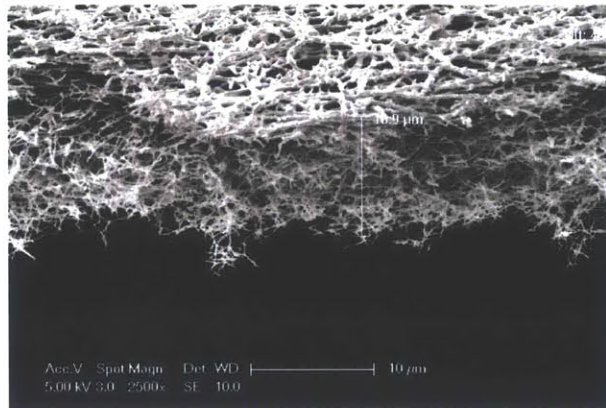


Figure 3.11: SEM Image of Freestanding Nickel Nanonetwork Cutaway

Figure 3.12 is the EDX of a nickel sample. From this figure, Ni is present at 95%. Therefore, the nanowire mineralization resulted in very pure nickel nanowires with little nickel oxide formation.

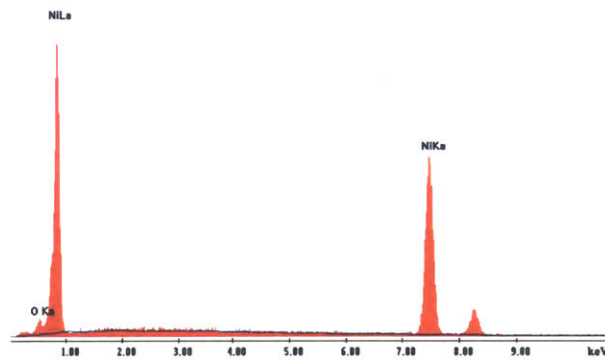


Figure 3.12: EDX of Nickel Nanonetwork

# Chapter 4

## Discussion and Conclusion

### 4.1 Overview

Mineralized hydrogels were successfully created with copper and nickel nanowires. Control of the hydrogels and nanowires will give this research broader applications. This chapter discusses different ways to control hydrogels and nanowires and limitations of the techniques used. Finally, suggestions for future research towards creating microbatteries are stated.

### 4.2 Hydrogel Control

#### 4.2.1 Porosity

The porosity of the hydrogel was relatively constant throughout the gel, except where phage was in contact with a substrate. Pore size was on the order of 100 nm - 1  $\mu$ m throughout the gels. Pore size is important, since metals experience large volume change during lithiation[24]. Void space must exist in order to let nanowires swell and contract while maintaining electrical connectivity. Pore size is also an inverse measurement of the phage density. To control pore size, different phage concentrations can be used. Phage concentrations of

$3 \times 10^{13}$  pfu/mL and lower generated hydrogels that were not mechanically stable, placing a lower bound on the phage concentrations for manipulable hydrogels.

### **4.2.2 Thickness**

Hydrogels were created at a variety of thickness, from a few  $\mu\text{m}$  up to 2 mm in height for fixed hydrogels. Freestanding hydrogels were created with thicknesses of up to 5 mm. The thickest hydrogels experienced the same mechanical stability as thinner hydrogels, suggesting that stable hydrogels of even greater height can be created. Scaling of the hydrogel in the z-direction provides control of total electrode mass post-mineralization for a given footprint. Increased height will necessitate better mineralization control on the interior of the hydrogel.

## **4.3 Mineralization Control**

The nanowire thickness is controllable with different mineralization conditions. Two factors greatly influenced the mineralization rate: the diffusion front of the reducing agent and the hydrogen gas evolution.

### **4.3.1 Diffusion Fronts**

Diffusion of ions into the hydrogel was complicated by the E3 phage. The phage hydrogel was still highly charged at pH 7 due to E3 terminal groups which provides an overall negative charge. The charged nature of the hydrogel results in an electric double layer. The small pore size of the hydrogel means that diffusion of charged species, such as metal ions and DMAB, is constrained. To overcome part of the diffusion front issue an ELD- solution was used, composing of the metal ion, a stabilizer, and a buffer. The ELD- solution was used to permeate the gel with a concentration of the metal ion so that only the reducing agent diffusion front controlled the mineralization. A high concentration of reducing agent was used

in order to force the charged reducing agent into the hydrogel where it would mineralize the interior.

### **4.3.2 Hydrogen Gas Evolution**

Hydrogen gas evolution provided the other complication to mineralization. As hydrogen gas bubbles formed around nanowires, the nanowires and phage encapsulated inside the bubble were unable to further mineralize due to lack of aqueous ion diffusion in gas. This issue was especially prevalent in the interior of the hydrogel, where gas bubbles filled void space and often did not detach from the hydrogel. Glycine was used in ELD solutions to stabilize the metal ions, decreasing reactivity to let some nucleation occur on all phage surfaces before large hydrogen gas bubbles formed.

## **4.4 Scalability of Electrodes**

Hydrogels were created and mineralized over a variety of length scales. The smallest hydrogels were no more than 20  $\mu\text{m}$  by 20  $\mu\text{m}$ . The largest were a circle of diameter 8 mm. The whole range of micron-scale to millimeter-scale is capable of supporting these mineralized electrodes. The wide range of possible sizes will be useful in finding a host of different applications for microbatteries because microelectronics could be made with microbatteries size-tailored for each device.

## **4.5 Future Directions**

### **4.5.1 Battery Testing**

Future directions of this work include testing the fabricated electrodes for their charging and discharging characteristics. Additionally, tunneling electron microscopy and X-ray diffrac-

tion should be used to determine the exact elemental makeup and phase of the pure metal nanowires. Additional types of nanowires should be mineralized and their battery characteristics tested. Once electrodes can be made to the proper size, porosity, and other specifications, the fabrication of whole batteries of variable sizes can be tested. The nanowire network should operate well as an electrode because of the porosity, which will provide space for volume changes due to lithiation, and high surface area, which will increase the rate of lithiation.

### **4.5.2 Mechanical Testing**

The 3D phage hydrogel is an important scaffold that can be used on projects outside of battery electrodes. To better understand the properties of this material, mechanical testing should be done using compression-based AFM and nanoindentation. This material has proven to be stable in a dried nanonetwork configuration of phage. Using the phage hydrogel as a mechanical material will improve the overall charge per mass ratio of batteries. Hydrogel-based electrodes that have mechanical rigidity will require less external battery housing, saving weight and volume.



# Bibliography

- [1] Mui, S.C.; Trapa, P.E.; Huang, B.; Soo, P.P.; Lozow, M.I.; Wang, T.C.; Cohen, R.C.; Mansour, A.N.; Mukerjee, S.; Mayes, A.M.; Sadoway, D.R., "Block Copolymer-Templated Nanocomposite Electrodes for Rechargeable Lithium Batteries," *J Electrochem Soc*, Vol. 149, pp. A1610-A1615, (2002).
- [2] Cassagneau, T.; Fendler, J.H., "High Density Rechargeable Lithium-Ion Batteries Self-assembled from Graphite Oxide," *Adv Mater*, Vol. 10, pp. 877-881 (1998).
- [3] Humble, P.H.; Harb, J.N.; LaFollete, R., "Microscopic Nickel-Zinc Batteries for Use in Autonomous Microsystems," *J Electrochem Soc*, Vol. 148, pp. A1357-A1361, (2001).
- [4] Lee, K.B.; Lin, L., "Electrolyte-based on Demand and Disposable Microbattery," *J Microelectromech Syst*, Vol. 12, pp. 840-847, (2003).
- [5] Wang, C.; Taherabadi, L.; Jia, G.; Madou, M.; Yeh, Y.; Dunn, B., "C-MEMS for the Manufacture of 3D Microbatteries," *Electrochem Solid-State Letters*, Vol. 7, pp. A435-A438, (2004).
- [6] Chamran, F.; Yeh, Y.; Min, H.S.; Dunn, B.; Kim, C.J., "Fabrication of High-aspect-ratio Electrode Arrays for Three Dimensional Microbatteries," *J Microelectromech Syst*, Vol. 16, pp. 844-852, (2007).
- [7] Keren, K.; Berman, R.S.; Buchstab, E.; Sivan, U.; Braun, E., "DNA-Templated Carbon Nanotube Field-Effect Transistor," *Science*, Vol. 302, pp. 1380-1382, (2003).
- [8] Braun, E.; Eichen, Y.; Sivan, U.; Ben-Yoseph, G., "DNA-Templated Assembly and Electrode Attachment of a Conducting Silver Wire," *Nature*, Vol. 391, pp. 775-778, (1998).
- [9] Tseng, R.J.; Tsai, C.; Ma, L.; Ouyang, J.; Ozkan, C.S.; Yang, Y., "Digital Memory Device based on Tobacco Mosaic Virus Conjugated with Nanoparticles," *Nature Nanotech*, Vol. 1, pp. 72-77, (2006).
- [10] Royston, E.; Ghosh, A.; Kofinas, P.; Harris, M.T.; Culver, J.N., "Self-assembly of Virus-structured High Surface Area Nanomaterials and Their Application as Battery Electrodes," *Langmuir*, Vol. 24, pp. 906-912, (2008).

- [11] Nam, K.T.; Wartena, R.; Yoo, P.J.; Liau, F.W.; Lee, Y.J.; Chiang, Y.-M.; Hammond, P.T.; Belcher, A.M., "Stamped Microbattery Electrodes based on Self-assembled M13 Viruses," *PNAS*, Vol. 105, pp. 17227-17231, (2008)
- [12] Kay, B.K.; Wynter, J.; McCafferty, J., *Phage Display of Peptides and Proteins: A Laboratory Manual*, Academic Press Inc.; San Diego, CA (1996).
- [13] Flynn, C.E.; Lee, S.-W.; Peelle, B.R.; Belcher, A.M., "Viruses as Vehicles for Growth, Organization and Assembly of Materials," *Acta Materialia*, Vol. 51, pp. 5867-5880, (2003).
- [14] Lee, Y.J.; Lee, Y.; Oh, D.; Chen, T.; Ceder, G.; Belcher, A.M., "Biologically Activated Noble Metal Alloys at the Nanoscale: For Lithium Ion Battery Anodes," *Nano Letters*, Vol. 10, pp. 2433-2440, (2010).
- [15] Yoo, P.J.; Nam, K.T.; Qi, J.; Lee, S.-W.; Park, J.; Belcher, A.M.; Hammond, P.T., "Spontaneous Assembly of Viruses on Multilayered Polymer Surfaces," *Nature Materials*, Vol. 5, pp. 234-240, (2006).
- [16] Nam, K.T.; Kim, D.-W.; Yoo, P.J.; Chiang, C.-Y.; Meethong, N.; Hammond, P.T.; Chiang, Y.-M.; Belcher, A.M., "Virus-Enabled Synthesis and Assembly of Nanowires for Lithium Ion Battery Electrodes," *Science*, Vol. 312, pp. 885-888, (2006).
- [17] Lee, Y.J.; Belcher, A.M., "Nanostructure Design of Amorphous FePO<sub>4</sub> Facilitated by a Virus for 3 V Lithium Ion Battery Cathodes," *J Mater Chem*, Vol. 21, pp. 1033-1039, (2011).
- [18] Lee, S.Y.; Royston, E.; Culver, J.N.; Harris, M.T., "Improved Metal Cluster Deposition on a Genetically Engineering Tobacco Mosaic Virus Template," *Nanotechnology*, Vol. 16, pp. S435-S441, (2005).
- [19] Gerasopoulos, K.; McCarthy, M.; Royston, E.; Culver, J.N.; Ghodssi, R., "Nanostructured Nickel Electrodes Using the Tobacco Mosaic Virus for Microbattery Applications," *J Micromech Microeng*, Vol. 18, pp. 1-8, (2008).
- [20] Dujardin, E.; Peet, C.; Stubbs, G.; Culver, J.N.; Mann, S., "Organization of Metallic Nanoparticles Using Tobacco Mosaic Virus Templates," *Nano Letters*, Vol. 3, pp. 413-417, (2003).
- [21] Lee, S.Y.; Culver, J.N.; Harris, M.T., "Effect of CuCl<sub>2</sub> Concentration on the Aggregation and Mineralization of Tobacco Mosaic Virus Biotemplate," *J Colloid Interface Sci*, Vol. 297, pp. 554-560, (2006).
- [22] Migneault, I.; Dartiguenave, C.; Bertrand, M.J.; Waldron, K.C., "Glutaraldehyde: Behavior in Aqueous Solution, Reaction with Proteins, and Application to Enzyme Crosslinking," *BioTechniques*, Vol. 37, pp. 790-802, (2004).

- [23] Lee, S.-W.; Belcher, A.M., "Virus-based Fabrication of Micro- and Nanofibers Using Electrospinning," *Nano Letters*, Vol. 4, pp. 387-390, (2004).
- [24] Chan, C.K.; Peng, H.; Liu, H.; McIlwrath, K.; Zhang, X.F.; Huggins, R.A.; Cui, Y., "High-Performance Lithium Battery Anodes Using Silicon Nanowires," *Nature Nanotechnology*, Vol. 3, pp. 31-35, (2005).